# VERIFICATION OF SSI EFFECT THROUGH THE EARTHQUAKE OBSERVATION

**KUNIAKI YAMAGISHI**

*Technical Research Institute, Mitsui Construction Co., LTD.*
*518-1, Komaki, Nagareyama-shi Chiba-ken.*
*E-mail : yamagishi@mcc48.mcc.co.jp*

**A workshop**
**"CHARACTERISTICS OF SEISMIC MOTION OF THE BUILDING AND GROUND"**
**in BRIC**

*Members are shown at the last page of the paper*

**ABSTRACT**

Empirical studies to verify the SSI effect through the earthquake observation are carried out. A workshop "Characteristics of seismic motion of the building and ground" organized since 1998 have investigated SSI effect through seismic observation data the members own. Investigating Fourier spectral ratios (basement or 1st floor / ground, and top floor / ground), relationship of the peak acceleration between ground and basement or 1st floor, and elongation of the first modal periods by flexible-base system, comparisons with the characteristics of SSI effect at each sites and with the provision are made.

**Keywords** Soil Structure Interaction, Earthquake Observation, Fourier Spectral ratio, Input Loss of Earthquake Motion

## INTRODUCTION

With rapid progress and advances in recording technology and reduction cost for installing the instruments, tremendous number of strong motion records of recent large earthquake have been obtained and released in Japan. The government, universities and private enterprises especially related to infrastructure like railroads, gas and electric power, have carried out many observations, and most of them are installed on ground. In order to design seismic loads properly it is important to understand not only characteristics of the strong ground motion, but also actual building behaviors subjected to seismic ground motion with SSI effect. To evaluate SSI effect through earthquake observation, it is necessary to employ simultaneous observations both in building and ground. But there are few simultaneous observation systems in Japan for the time being.

As for the seismic design code, the building code in US such as ATC-3 and FEMA302 involves the SSI effect explicitly. On the other hand, in Japan the SSI effect has just been taken explicitly in the latest structural design code called "Calculation procedure on response and limit strength" adopted in the revision Building Standard Law in 2000.

There is a pressing need to gather earthquake motion records and analyze them to evaluate the SSI effect empirically for various buildings and seismic intensities. So the authors have established a workshop "Characteristics of seismic motion of the building and ground" in BRIC (Building Research Institute Consortium) committee, which is a collaboration of BRI and laboratories of private companies in the North Kanto area since 1998. In the workshop, various seismic observation data members offer have been examined and investigated the qualitative and quantitative SSI effect. The data related to seismic motions are peak ground accelerations, peak acceleration of the foundation and smoothed Fourier amplitude spectra.

This paper describes the outline of the structural features and recording systems for 8 buildings and discusses the SSI effects of those buildings through the analyzing Fourier spectral ratios (basement or 1st floor / ground, and top floor / ground), relations of maximum acceleration between ground and building basement or 1st floor, elongation of the natural periods. A comparison was further made between collected data and FEMA302 assigned parameter values.

## OUTLINE OF EARTHQUAKE OBSERVATAION AND STRUCTURAL CHARACTERISTTICS

Figure 1 shows the locations of eight sites referred in this study. The simultaneous observations in structure and free-field have been conducted at seven sites (AOB is for structure only). In most of the sites, the sensors are installed in the surrounding ground at various depth levels, and are also installed in the structure at some floor and in the pile. All the structures are instrumented with the digital accelerometers.

The northernmost site is AOB (at Miyagi Prefecture) and the westernmost and the southernmost one is TKM (at Osaka Prefecture), most of the sites are located in North Kanto area, among then three sites (ANX, KII, TDI) are located at Tsukuba city in Ibaraki Prefecture. Table 1 shows the outline of the structures at eight different sites, whose shape, height, foundation of structures and seismic structural type varies. According to structural type, KII and AOB employs seismic isolation systems, ANX is steel reinforced concrete frame structure, HRM is CFT (Concrete Filled Tube) structure, and all of the structure except ANX and HRM are conventional reinforced concrete frame structures. According to use of the structure four of them are used as laboratories, three used as housing which are high-rise buildings, height of which are larger than 60m.

Foundations of most of the structures in Japan are supported on average soil deposit, however that of MST site is relatively softer and AOB is harder than other sites, and all of the structures employ pile foundations except ANX and AOB which employ mat foundations. Further precise description of structures, recording systems and soil condition are shown Appendix at the end of this paper.

## OBSERVED RECORDS

Figure 2 shows epicenters of the events observed on the sites from 1992 to 2000 and Figure 3 shows frequencies of observed peak ground acceleration (PGA) dividing into the longitudinal and transverse direction of the structure. Most of the PGAs are less than 1 $m/s^2$, and most of the records show the PGA around 0.1 $m/s^2$. Distribution of magnitude and focal depth of the events are shown in Figure 4. The largest magnitude of all the events is M8.1 (Japan Meteorological Agency magnitude) occurred in 1994 called “East Off Shore Hokkaido”, but most of the data are for magnitude around 5 and the epicenters are located near each observation sites. So there are a few events for which more than two sites obtained records simultaneously. Judging from the frequencies for focal depth, most of the events occurred near the subduction zone where Pacific Ocean Plate and Eurasia Plate collies.

## VERIFICATION OF SSI EFFECT

### Analysis Procedure

The SSI effect is expressed as follows, (a) input loss of earthquake motion by the effect that basement restrict ground motions, (b) period elongation due to the flexible-base modal vibration, and (c) the change of damping ratio. It is so difficult to identify the damping ratios of the systems because of the lacking of necessary data that we mainly investigated about (a) and (c).

Fourier spectra are obtained by using FFT. After that it is smoothed by Parzen window with the bandwidth of 0.2Hz. Before passing FFT, data correction is carried out so that summation of all the data to be naught.

To investigate the input loss of earthquake motion, spectral ratios (the basement or $1^{st}$ floor / near ground surface) are calculated and averaged at each sites. Division to calculate the ratios is carried out after the Fourier spectra are smoothed. Comparing with each site, the normalized frequencies, which are the fixed-base natural modal frequencies, are used. The averaging of Fourier spectra is carried out before normalization though seismic motions change the standard frequencies to normalize and the increment frequencies.

To investigate the period lengthening ratio of flexible- to fixed-base of $1^{st}$ modal vibration, peak frequencies of the two spectral ratios, which are the ratio of spectra at the top to at near, ground surface and the ratio at the top to at the basement or $1^{st}$ floor are calculated. The former ratio expresses flexible-base $1^{st}$ modal frequency and the latter expresses fixed-base $1^{st}$ modal frequency. So calculated $1^{st}$ modal vibrations in this paper include rocking motions. To calculate them, least square method using fourth-order polynomial is used. Because the spectra and spectral ratios of the middle-rise structure are disordered on the other hand those of high-rise structure are clear. So evaluation of the middle-rise structure (especially more than 3.0Hz frequency) is less accurate than that of the other structures.

**Comparison of Free-Field and Foundation-Level Structural Responses**

A simple investigation of kinematic and inertial interaction effects can be made by comparing PGA of free-field and peak acceleration of foundation motions referred to as PFA (peak foundation acceleration) hereafter in this paper. Figure 5 shows the compared results of all the peak accelerations recorded simultaneously between on the surfaces of the ground and on the foundation dividing the results into longitudinal (L) and transverse (T) direction of the foundation. The slopes of the dotted and broken line obtained by linear regression are 0.74 for L and 0.60 for T respectively, and the average slope 0.66 is compatible value shown in Iguchi et al. (1998). Regarding the depth of foundation, the ratios (PFA/PGA) shown in Figure 6 are decreasing as the depth increase, and are under unity with depth is greater than 5.0m. Deserving special mention is that the PFAs are remarkably de-amplified relative to the free-field with seismic isolation system. The reason of this de-amplification in seismic isolation system is coincident to that the structure will not to excite high-order modal vibration, the inertial force of which is affected on the foundation-level acceleration. Figure 7 shows the relationship foundation radii and the ratios (PFA/PGA), and indicates the ratios decreasing as the foundation radius becomes larger.

**The Input Loss of Earthquake Motion**

Spectral ratios at seven sites are shown in Figure 8. The range of ratios is decreasing as the frequency becomes higher because kinematic interaction is dominated in high frequency domain. Most of the ratios have the same fluctuations and some of the ratios are greater than unity at some frequencies. TKM, TKI and TDI sites have peaks of the ratios in relatively systematic at 3 on the normalized frequencies. Thinking the higher order modal frequency of the structure, which is permitted only shearing deformation, higher modal frequency will appear at the odd number times of the first modal frequency according to modal degrees, so the remarkable changes at 3 in Figures may be affected by the second order mode of the structures. The ratio of KII, which is seismic isolation structure, is beautifully decreasing with the increase of normalized frequency. Judging from the same manner of the structural vibration, the participation factor for the higher modes of seismic isolation system is so small that the peaks of ratio would not be appeared. ANX has mat foundation, whereas the foundation of all other structures are pile foundation, the higher order modal affection on the ratio of ANX is not seen clearly, and input loss of earthquake motion is relatively large. MST has a rugged ratio between at 1 to at 3 of normalized frequency, and the change of ratios for frequency is greater than other high-rise structures. In HRM the ratio seems to be smooth and flat, the location of the accelerometer is so close to the structure, the distance from the structure to the accelerometer is about 3m, that the structure will easily affect on the accelerometer.

**The Period Lengthening Ratio of Flexible-base to Fixed-Base**

Amplitude dependencies of the fixed-base natural 1$^{st}$ frequency is shown in left columns of Figure 9 grouping into the structural types, which are relatively squat, slender and seismic isolation system. The largest changes of the natural frequency with PGA are shown in two seismic isolation systems (AOB, KII) (Figure 9-(3) left), and the degree of declination of them is as same as one another. Secondarily large changes are shown in relatively squat structure (Figure 9-(1) left), especially in structures having shorter frequencies. The frequency change is not clear in slender structures, which were not subjected to so large excitation as far as this study is concerned.

Similarly, the relationship between PGA and period lengthening ratio ($T/T_0$) is shown in right columns of Figure 9, there is a significant scatter in the data of squat structure (Figure 9-(1) right), and is not so correlative to the PGA. On the other hand in seismic isolation structure the change of $T/T_0$ is not appeared with the PGA increase (Figure 9-(3) right). So, the parameter $T/T_0$ is not so sensitive for PGA

Analytical formulations for SSI are numerous, and analytical method and numerical approaches like a finite element analysis procedures are taken for many years. From these research activities some of the simplified dimensionless parameters $r\omega/Vs$ for example is used for the explanation of SSI effect. However the actual condition with regard to the structure and surrounding ground is so complicated, such as complexity in shape and in plan of the foundation, effect of group piles and local discontinuity like a gap between foundation and soil. To take SSI effect into consideration to design a question will occur how many parameters we need to take into consideration for SSI effect, and on the contrary, what is the most sensitive parameter and what type of structure is (or not) affected by the SSI effect qualitatively. So to investigate the sensitivities of the parameters to the SSI effect especially period lengthening ratio ($T/T_0$) through the observations, the correlation coefficients of $T/T_0$ to various parameters are calculated and the result is shown in Figure 10. In this figure the factors are arranged in the order of magnitude in correlation coefficient, then the dimensionless parameter $r\omega/Vs$, in which r is

foundation radius, $\omega$ is circular frequency and Vs is shear wave velocity of the soil, is the most correlated parameter for ratio $T/T_0$ the correlation coefficient of which is 0.67. And the parameters, which have relatively close correlation with $T/T_0$, are related to the frequency of the structure and soil and the shape of the structure and foundation. On the other hand, acceleration level and the parameters related to the event are not related to $T/T_0$.

**COMPARISON TO THE FEMA 302**

To take SSI effect into account in design, it is necessary to evaluate the actual SSI effect. Method to evaluate SSI effect assigned in FEMA302 is almost the same as ATC-3 which is based on theoretical results and the results of numerical analysis. So applying it to the structures mentioned in this paper, it would be able to compare the empirical results with theoretical ones. Here comparison about period lengthening ratio ($T/T_0$) is shown.

According to FEMA302, $T/T_0$ is expressed as follows:

$$\frac{T}{T_0} = \sqrt{1+\frac{k_0}{K_y}\left(1+\frac{K_y h^2}{K_r}\right)} \tag{1}$$

in which $k_0$ is the stiffness of the structure for fixed base condition, $K_y$ and $K_r$ are lateral and rocking stiffness of the foundation, respectively, h is the effective height of the structure. For circular mat foundation supported at the surface of a homogeneous half-space, stiffness $K_y$ and $K_r$ are expressed as follows:

$$K_y = \frac{8Gr}{2-\upsilon} \tag{2}$$

$$K_r = \frac{8Gr^3}{3(1-\upsilon)} \tag{3}$$

in which G and $\nu$ are the shear modulus and the Poisson's ratio of the soil, respectively, and r is the radius of foundation. Essentially period-dependency factor must be multiplied in Eq.(2) and (3), it is sufficiently accurate for practical purposes to use them. For embedded foundation $K_y$ and $K_r$ are expressed as follows:

$$K_y \approx \frac{8Gr}{2-\upsilon}\left[1+\frac{2}{3}\left(\frac{d}{r}\right)\right] \tag{4}$$

$$K_r \approx \frac{8Gr^3}{3(1-\upsilon)}\left[1+2\left(\frac{d}{r}\right)\right] \tag{5}$$

in which d is the depth of embedment.

When the foundation rests on a stratum of soft soil underlain by a much stiffer, rock-like deposit $K_y$ and $K_r$ are expressed as follows:

$$K_y \approx \frac{8Gr}{2-\upsilon}\left[1+\frac{2}{3}\left(\frac{d}{r}\right)\right]\left[1+\frac{1}{2}\left(\frac{r}{Ds}\right)\right]\left[1+\frac{5}{4}\left(\frac{d}{Ds}\right)\right] \tag{6}$$

$$K_r \approx \frac{8Gr^3}{3(1-\upsilon)}\left[1+2\left(\frac{d}{r}\right)\right]\left[1+\frac{1}{6}\left(\frac{r}{Ds}\right)\right]\left[1+0.7\left(\frac{d}{Ds}\right)\right] \tag{7}$$

in which Ds is the total depth of the stratum.

Though these equations are applied to the mat foundation, the values of $K_y$ and $K_r$ for pile foundation should be determined from field tests or proper computations. As the evaluation of $K_y$ and $K_r$ for pile foundation is not discussed in this paper, so the stiffnesses, especially $K_r$, would be underestimated for pile foundation.

The evaluation method using Eq. (2) and (3) may be called as Method-1 in this paper, and that using Eq.(4) and (5) as Method-2, and that using Eq. (6) and (7) as Method-3, respectively. The Poisson's ratio of soil $\nu$ is considered to be 0.475, Ds to be the depth that the layer of Vs about 400m/s appears, and shear velocity Vs to be average of the shear velocities weighted in thickness of soil layers as far as the depth of Ds, respectively.

The Figure 11 shows the relationship of the $T/T_0$ between observation (symbols) and Method-1 (mesh) that is the simplest form of all three methods. Dependency on the parameters $r\omega/Vs$ and L/r based on theory is well

appeared to the observation results, and $T/T_0$ is increasing as the $r\omega/Vs$ and L/r increase. In middle rise structures, $T/T_0$ of TKI (height is 13m) and TDI (height is 18m) is larger than that of ANX (height is 25m). The primary reason for the difference is due to that middle rise structure would be the significant difference of natural frequencies from ANX to TKI and TDI, the frequency ratio is ANX:TKI:TDI=1.0:2.1:3.2. So dimensionless parameter $r\omega/Vs$ which contains natural frequency is decreasing with TKI, TDI and ANX in order. $T/T_0$ of high rise and seismic isolation structure does not change so much because the parameters $r\omega/Vs$ are relatively low. So low and middle-rise structure will be likely subjected to the increase of period lengthening ratio of SSI effect, and high-rise structure will not be expected so much. Further, seismic isolation structure will not also be expected so much because of the low frequency in spite of its small height.

Figure 12 shows the relationship between $r\omega/Vs$ and the ratio of analytical results to observed ones. Evaluation by the Method-1 is relatively larger than observed results, and evaluation by the Mothod-3 generally coincides except TKI and TDI, which are underestimated. So the effect of embedment and the stiffening effect, which is caused by the layered half space of the soil are important to evaluate the SSI effect. Further the evaluation of $K_r$ involving the axial stiffness increase with piles is lacking in this study, so $T/T_0$ will be close to unity.

## CONCLUSIONS

Input loss of earthquake motion and period lengthening of SSI effect were investigated through the earthquake observation. Using the data of peak ground acceleration, peak acceleration of foundation and smoothed Fourier spectra, some conclusions are obtained as follows.

-The input loss of earthquake motion was observed clearly at all sites. The spectral ratio ($1^{st}$ floor or basement / ground surface) is decreasing with higher frequency due to kinematic interaction, and is changing near the natural modal frequencies due to inertial interaction. Especially in seismic isolation structure the influences of the inertial interaction effect at higher modes are relatively small.

-The ratio of peak acceleration of foundation to peak ground acceleration of all the data is about 0.66, which value is compatible with other previous results, and is decreasing as the foundation depth and radius is increasing. In seismic isolation structure the ratio is remarkably de-amplified compared with its foundation depth and radius.

-Period lengthening ratio is larger in middle-rise structure than in high-rise structure. Natural modal frequency is dependent on the level of acceleration remarkably in seismic isolation structures. The most sensitive factor that contributes to period lengthening ratio is the dimensionless parameter $r\omega/Vs$.

-Empirical results coincide with the results by the FEMA302 method, and it is necessary to consider the effect of embedment and the stiffening effect, which is caused by the layered half space of the soil.

References:

NEHRP Recommended provisions for seismic regulations for new buildings and other structures (1998).Federal Emergency Management Agency

Stewart, J.P. (1998). "Empirical assessment of soil-structure interaction effects from strong motion recordings," Proc. UJNR workshop Soil-Structure Interaction, 7-1 to 7-21.

Iguchi, M. (1998). “State of the art on soil-structure interaction researches relating to recent strong earthquake in Japan,” Proc. UJNR workshop Soil-Structure Interaction, 1-1 to 1-17.

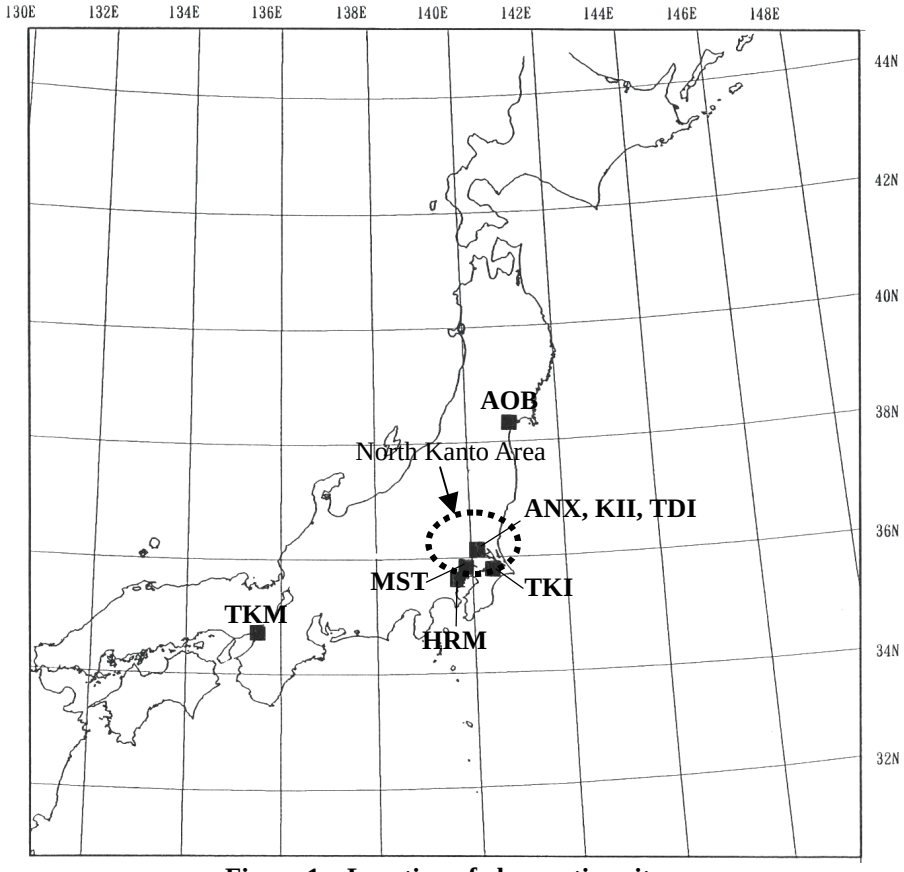


**Figure 1 Location of observation sites**

**Table 1 Outline of structures**

| | ANX | AOB | TKM | KII | TKI | TDI | MST | HRM |
|---|---|---|---|---|---|---|---|---|
| use of structure | laboratory | office | housing | laboratory | laboratory | laboratory | housing | housing |
| structural type | RC | RC | RC | RC | RC | RC | RC | CFT |
| base-isolation building | — | ○ | — | ○ | — | — | — | — |
| foundation type | Mat | Mat | CIPC Pile | CIPC Pile | PHC Pile | CIPC Pile | SC & PHC Pile | CIPC Pile DWF |
| height of structure | 25.0 m | 29.6 | 89.3 | 14.5 | 12.6 | 22.5 | 61.9 | 159. |
| foundation depth | 8.0 m | 4.5 | 8.5 | 3.2 | 1.8 | 1.8 | 4.6 | 15. |
| length of piles | — | — | 32.0 m | 12.0 | 15.5 | 13.0 | 55.6 | 19.0 |
| Vs: subsurface layers | 110～460 m/s | 345 | 140～330 | 160～290 | 120～300 | 120～484 | 100～300 | 110～380 |
| Vs: bearing stratum m/s | 500 m/s | 495 | 550 | 550 | 500 | 610 | 400 | 380 |
| accelerometer on the ground surface | GL-1.0m | — | GL-1.5m | GL-0.0m | GL-3.0m | GL-1.2m | GL- 1.0m | GL-1.0m |
| accelerometer on the foundation | B1F | SIB | 1F | SIB | 1F | 1F | 1F | B2F |

where RC: Reinforced Concrete structure, CFT: Concrete Filled Tube structure, Mat: Mat foundation, CIPC: Cast-in Place Concrete, SC: Steel pipe reinforced concrete, PHC: Pre-stressed high strength concrete, DWF: Diaphragm wall foundation, SIB: Seismic Isolation Basement

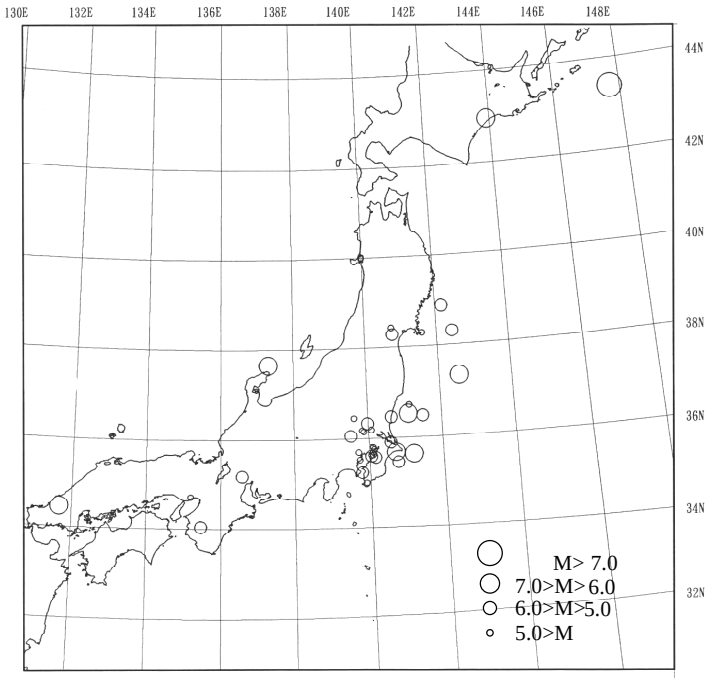


**Figure 2 Location of epicenters of analyzed events**

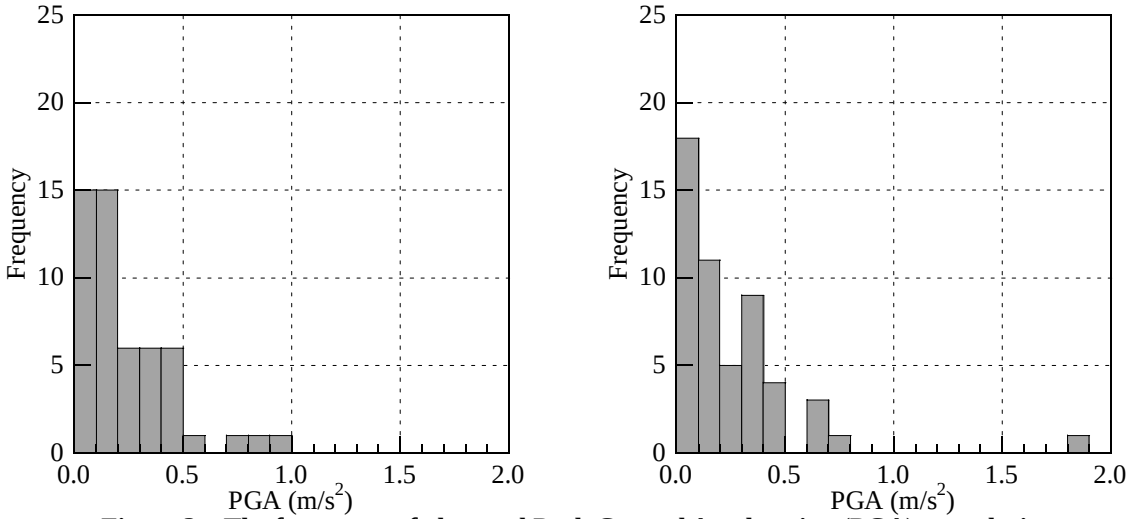


**Figure 3 The frequency of observed Peak Ground Acceleration (PGA) at each sites**

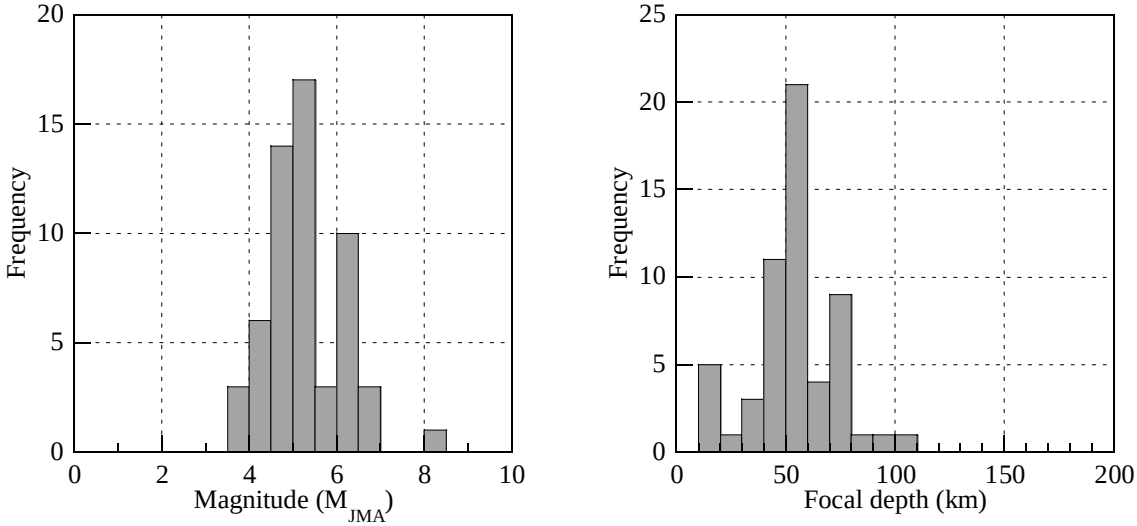


**Figure 4 The frequency of magnitude in JMA scale and focal depth**

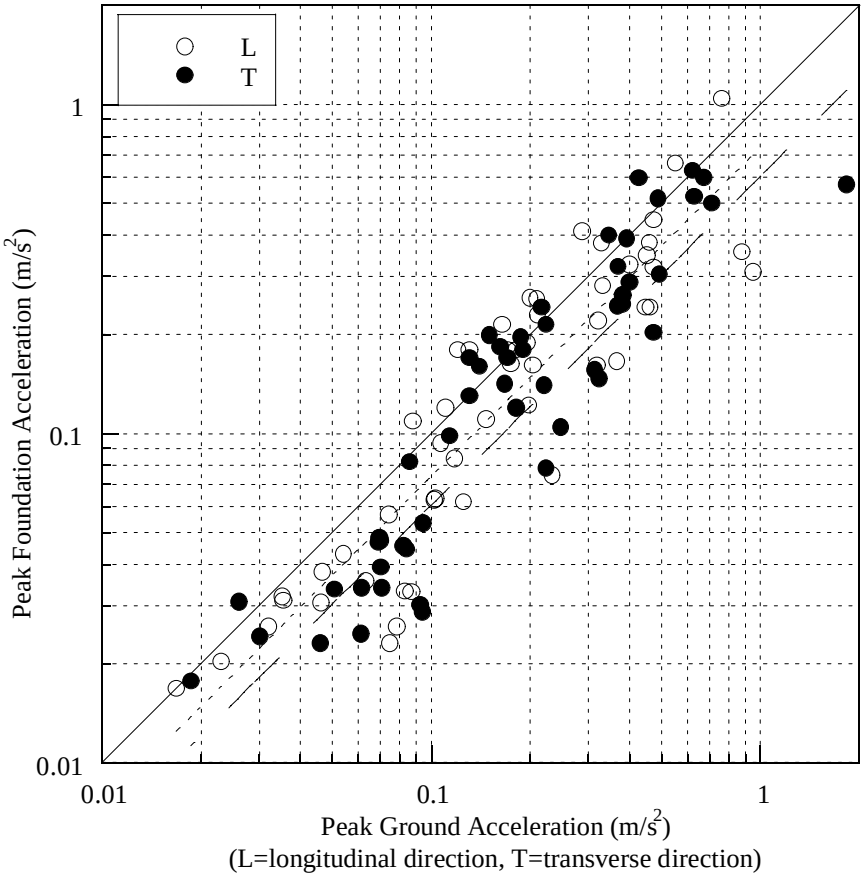


**Figure 5 Relationship between Peak Foundation Acceleration and Peak Ground Acceleration (dotted and broken line are regression line of Longitudinal and transverse direction, respectively)**

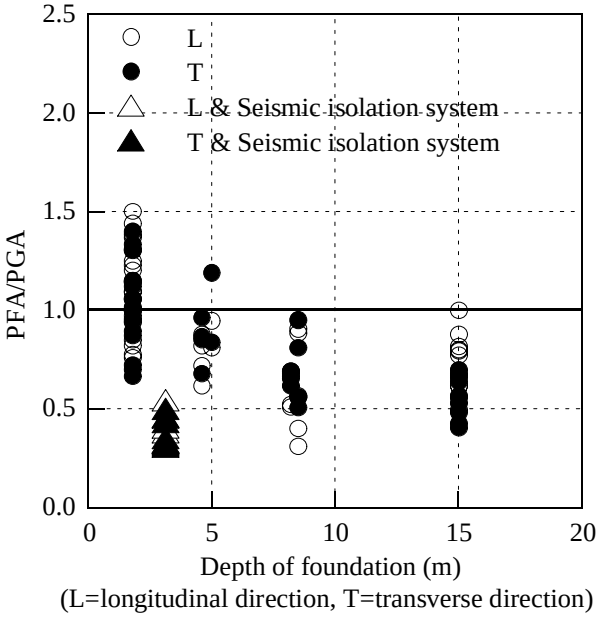


**Figure 6 Relationship between depths of foundation and PFA/PGA**

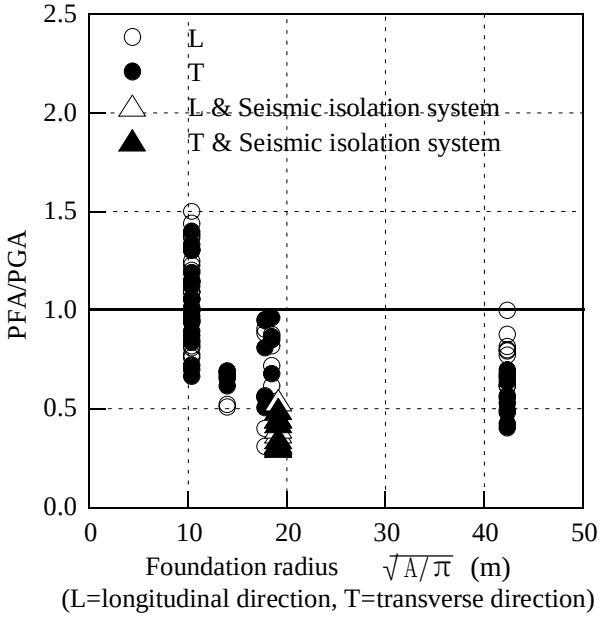


**Figure 7 Relationship between radii of foundation and PFA/PGA**

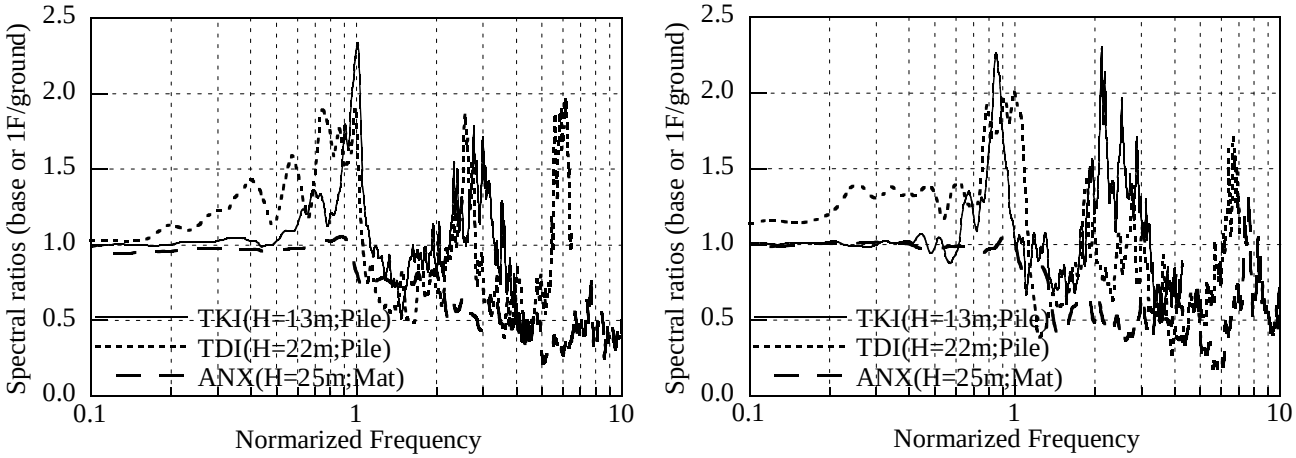


**(a) longitudinal direction** **(b) transverse direction**

**Figure 8-(1) Averaged spectral ratios between the basement (or 1st floor) and surface ground (middle-rise buildings)**

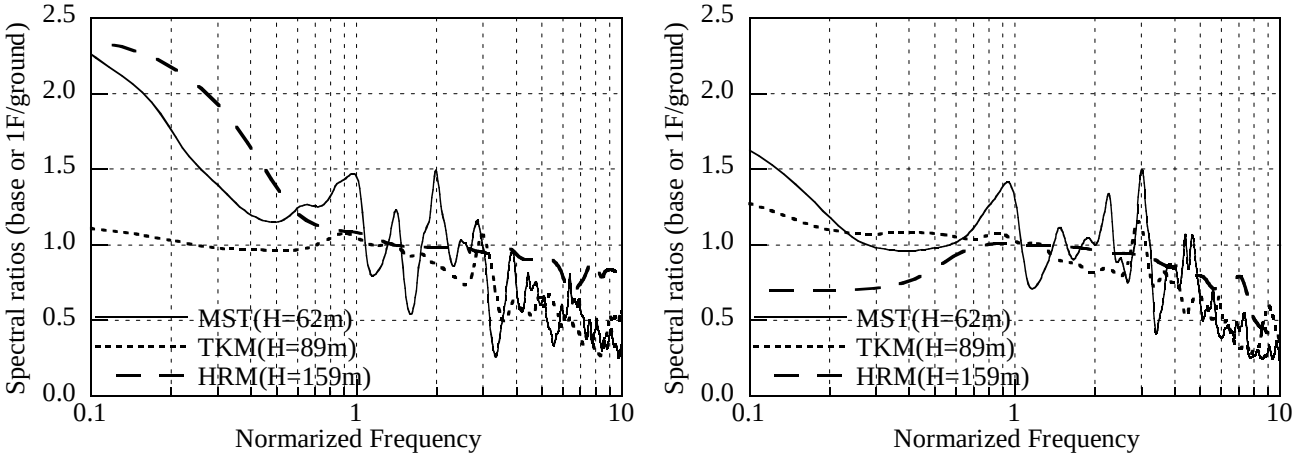


**(a) longitudinal direction** **(b) transverse direction**

**Figure 8-(2) Averaged spectral ratios between the basement (or 1st floor) and surface ground (high-rise buildings)**

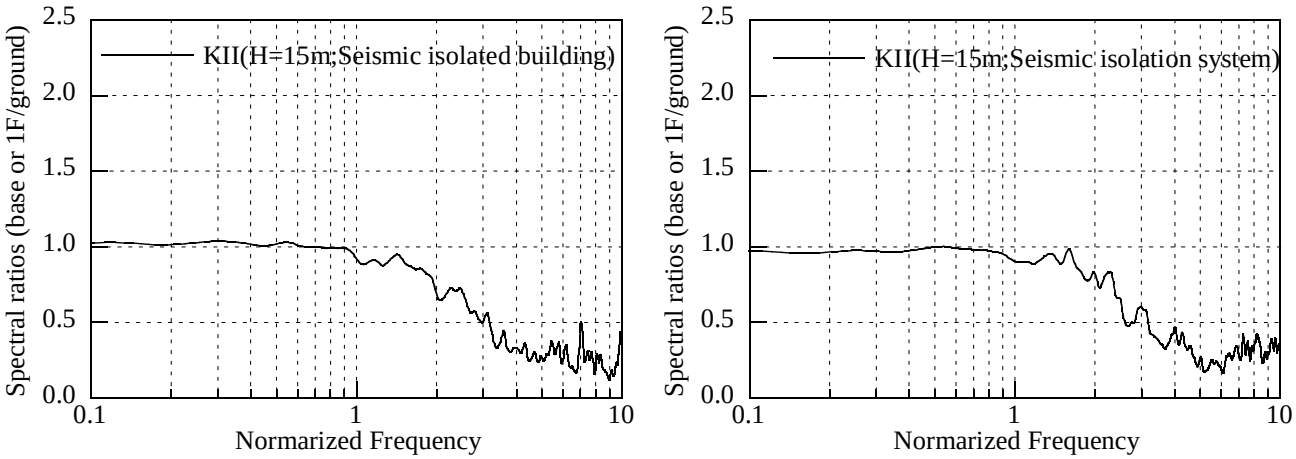


**(a) longitudinal direction** **(b) transverse direction**

**Figure 8-(3) Averaged spectral ratios between the basement (or 1st floor) and surface ground (seismic isolation structure)**

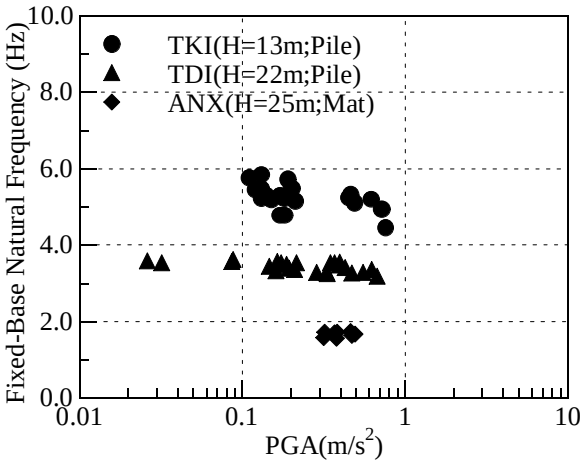


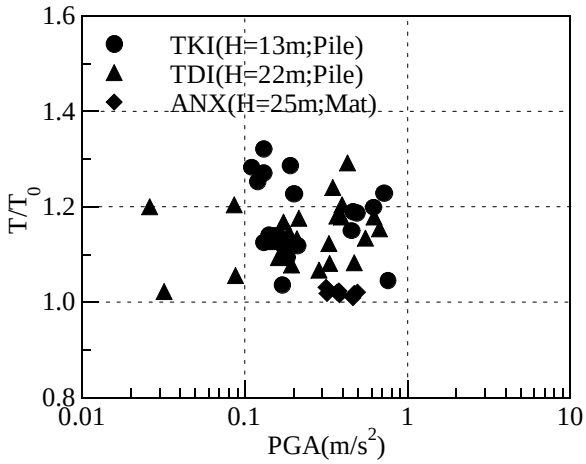


**(a) Fixed-base Natural frequency Vs. PGA** **(b) $T/T_0$ Vs. PGA**

**Figure 9-(1) Relationship between natural frequency of fixed-base building and PGA (middle-rise buildings)**

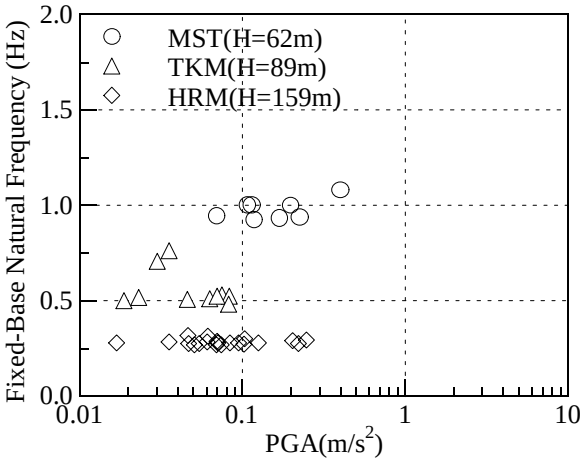


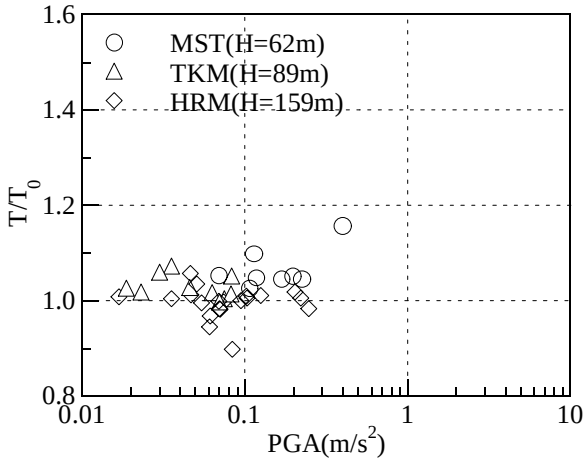


**(a) Fixed-base Natural frequency Vs. PGA** **(b) $T/T_0$ Vs. PGA**

**Figure 9-(2) Relationship between natural frequency of fixed-base building and PGA (high-rise buildings)**

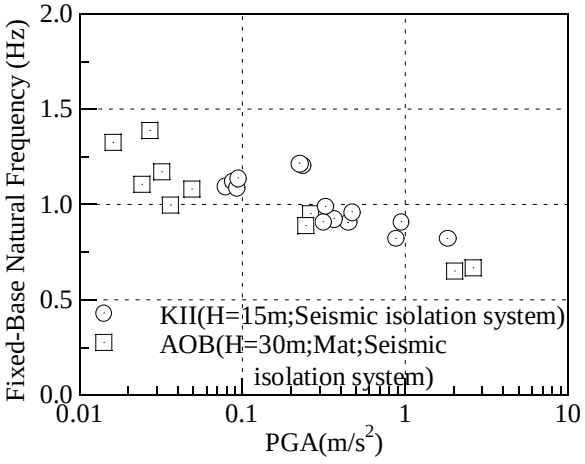


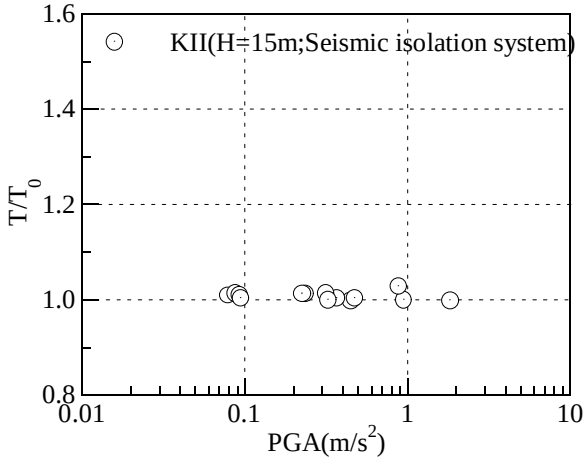


**(a) Fixed-base Natural frequency Vs. PGA** **(b) $T/T_0$ Vs. PGA**

**Figure 9-(3) Relationship between natural frequency of fixed-base building and PGA (seismic isolation buildings)**

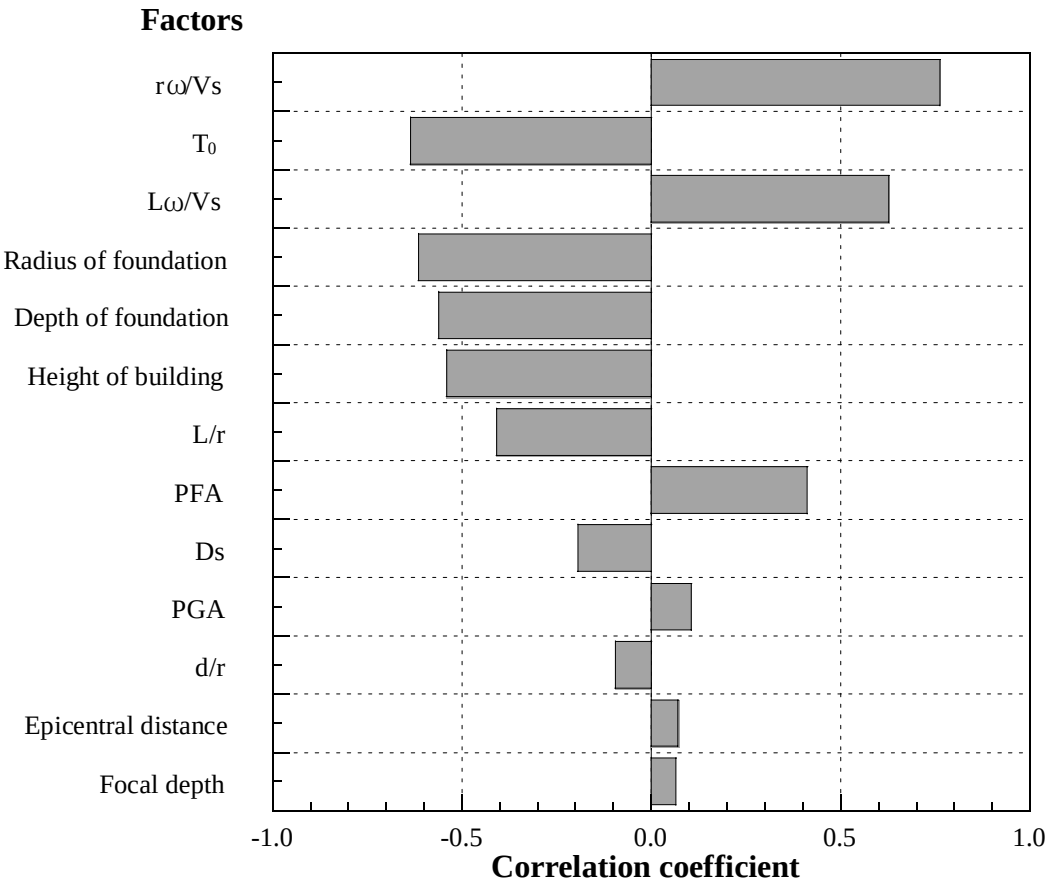


r : radius of foundation, d : depth of foundation, L : height of structure, Ds : total depth of the stratum
ω : circular frequency of fixed-base 1st modal vibration, $T_0$ : 1/ω,
PGA : peak ground acceleration, PFA : peak acceleration of foundation

**Figure 10 Correlation coefficients ( $T/T_0$ Vs. other factors)**

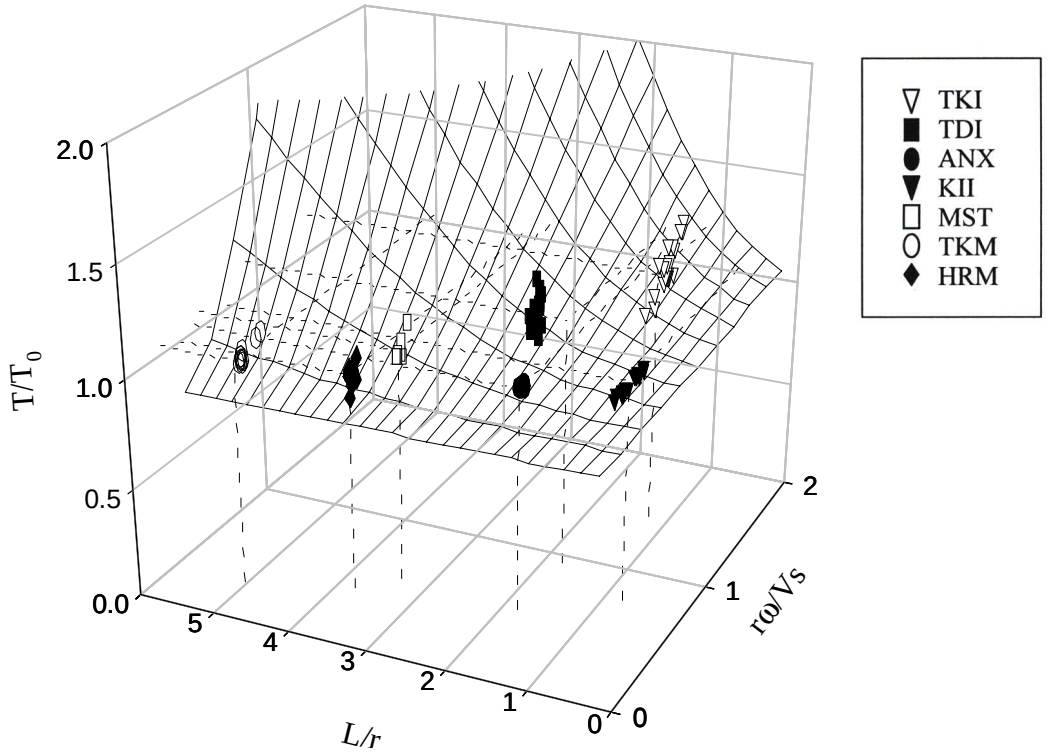


**Figure 11 The relationship of $T/T_0$ between observation and Method-1 (FEMA302)**

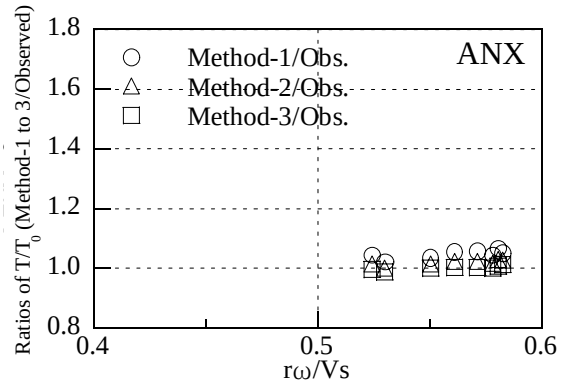


(a) ANX (height=25m; mat foundation)

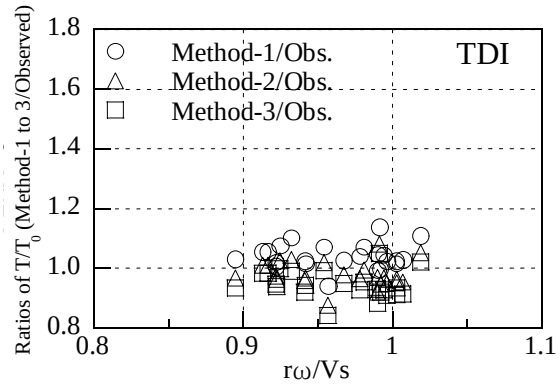


(b) TDI (height=22m; pile foundation)

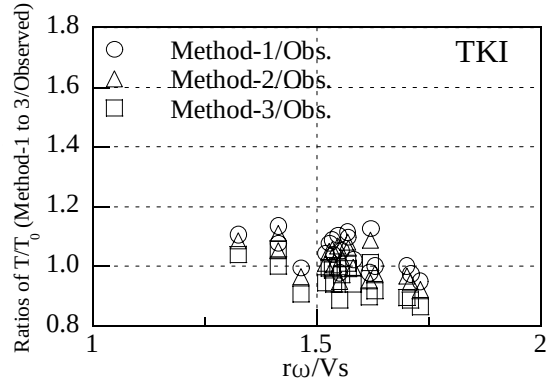


(c) TKI (height=13m; pile foundation)

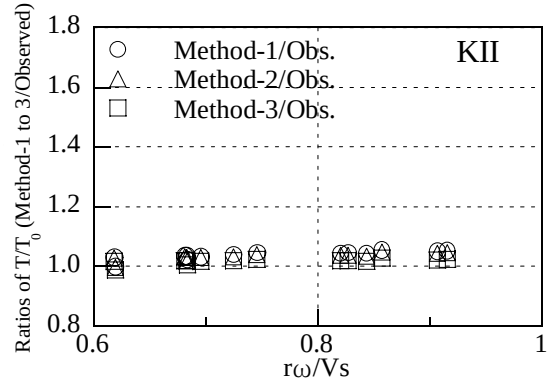


(d) KII (height=15m; pile foundation; seismic isolation structure)

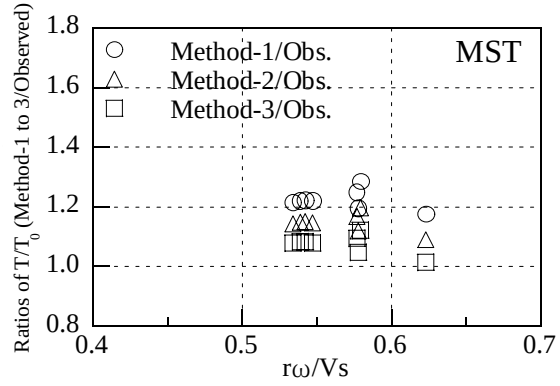


(e) MST (height=62m; pile foundation)

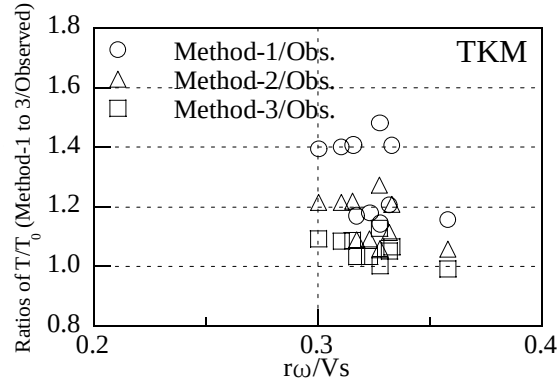


(f) TKM (height=89m; pile foundation)

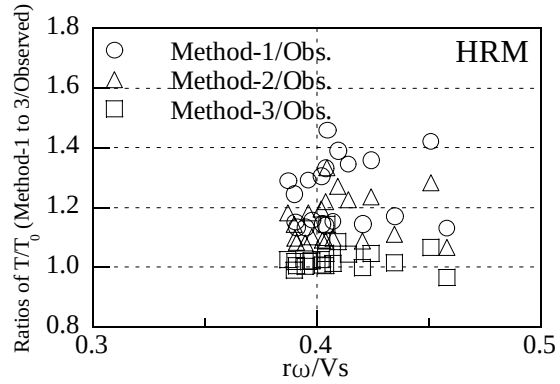


(g) HRM (height=159m; pile foundation)

**Figure 12 The Ratio of calculated period lengthening ratios to observed ones at each sites**

## APPENDIX ～ Outline of the observation sites ～

### 1. ANX

The building for accelerometer installation was completed in March 1998. The building has eight stories with single basement floor. Total building area is approximately 5,000m$^2$ and the building is supported by mat foundation on the clayey layer of 8.2m underground.

The sensors are installed with 11 locations (33 channels) in the building and 7 locations in the surrounding ground. Sensor configuration is shown in Figure A-1.1 and A-1.2. The farthest sensor on the ground is 100 meters away from the building, and the deepest sensor is set up 89 meters in depth. Three sensors are set up at the basement floor and the eighth floor in order to investigate torsional vibration.

Surface soil structure at ANX is shown in Table A-1.1, and the transfer functions for shear waves between ground surface and depths of 42m, 68m, and 88m are shown in Figure A-1.3. The figure shows common predominant frequencies of 2 to 4 Hz and 9 Hz.

All sensors are connected to the recording equipment at the observation room in the building. The system has 66-channel 24-bit A-D converters, a digital processing unit and 40 MB flash memory storage. PC cards are used as storage device and are directly processed by PC. Broad dynamic range and certain operation are ensured by the most up-to-date facilities.

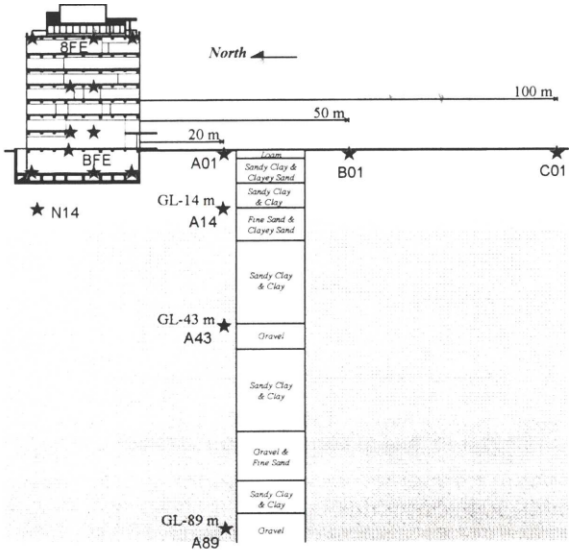


**Figure A-1.1 Vertical sensor configuration**

**Table A-1.1 Structure of surface soil layers**

| No. | $H$ (m) | $D$ (m) | $V_P$ (m/s) | $V_S$ (m/s) | $\rho$ (t/m$^3$) | Soil Type |
|---|---|---|---|---|---|---|
| 1 | 2.0 | 2.0 | 170 | 110 | 1.30 | Loam |
| 2 | 6.0 | 8.0 | 1430 | 200 | 1.30 | Sandy Clay & Clayey Sand |
| 3 | 6.0 | 14.0 | | 160 | 1.50 | Sandy Clay & Clay |
| 4 | 8.0 | 22.0 | 1630 | 260 | 1.80 | Fire Sand & Clayey Fine Sand |
| 5 | 6.0 | 28.0 | 1500 | 200 | 1.75 | Sandy Clay & Clay |
| 6 | 14.0 | 42.0 | 1570 | 270 | | |
| 7 | 6.0 | 48.0 | 1880 | 460 | 1.90 | Gravel |
| 8 | 8.0 | 56.0 | 1780 | 340 | 1.75 | Sandy Clay & Clay |
| 9 | 12.0 | 68.0 | 1690 | 290 | | |
| 10 | 12.0 | 80.0 | 1790 | 380 | 1.95 | Gravel & Fine Sand |
| 11 | 8.0 | 88.0 | 1600 | 280 | 1.75 | Sandy Clay & Clay |
| 12 | | | | *500* | *2.00* | Gravel |

$H$: Thickness, $D$: Depth, $V_P$: P-wave Velocity, $V_S$: S-wave Velocity, $\rho$: Density

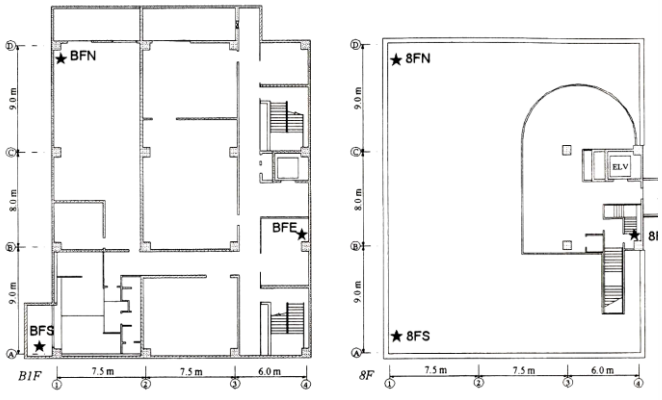


**Figure A-1.2 Sensor configuration at basement floor and 8th floor**

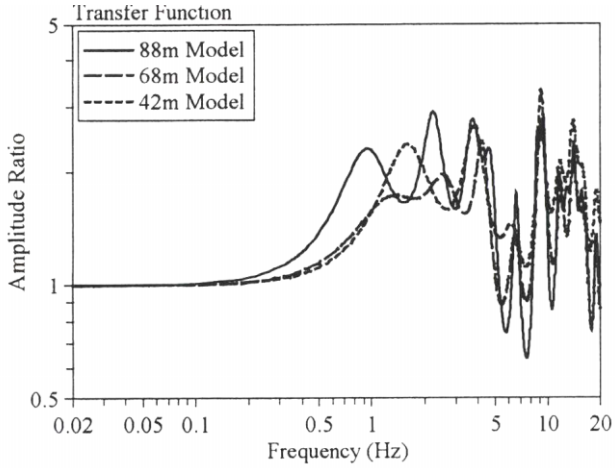


**Figure A-1.3 Transfer function of surface soil layers**

## 2. TKI

Figure A-2.1 shows the TKI site recording system. The building is three stories with one penthouse floor, reinforced concrete frames and floors with shear walls built in the moment resisting frames, and using the pile foundation (see Figure A-2.2 (a)). The diagram also shows the vertical view and the building scale of height of 12.6m, a maximum height of 16.0m. As the plane view in Fig. A-2.2(b), the shape of cross section is the rectangular of the longer side of 21m in 3 spans (X-direction) and the shorter side of 16m in 2 spans (Y-direction). Sensor configuration is shown in Figure A-2.2. 2 sensors set up in the ground at 3m and 31m in depth, 3 sensors set up on 1st floor and roof floor, respectively.

Surface soil structure at TKI is shown in Table A-2.1, and the transfer function for shear waves between ground surface and depths of 20m is shown in Figure A-2.3. The figure shows predominant frequency of 3.4Hz. The system has 24 channels, 16bit A/D converter, IC memory storage. The sampling frequency is 100Hz, the dynamic range is (+/-) 1G, and triggering logic disjunction (OR) of three components on the 31m ground level in depth.

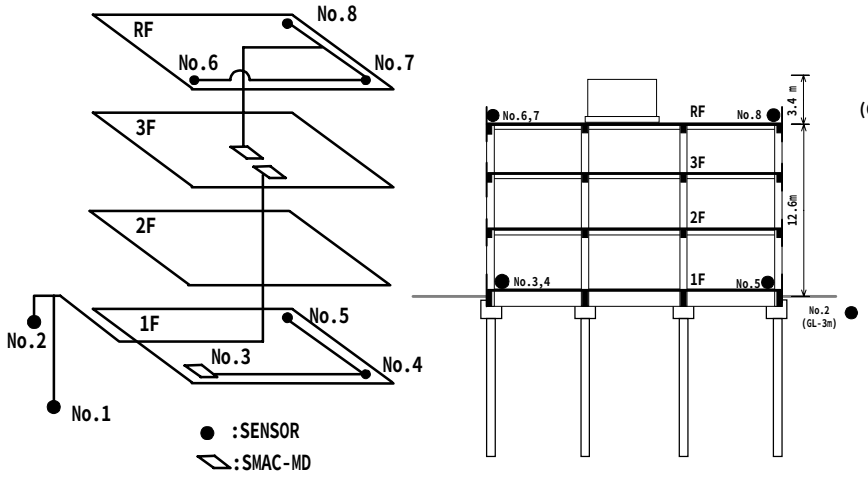


**Figure A-2.1: Schematic diagram of TKI site earthquake recording system**

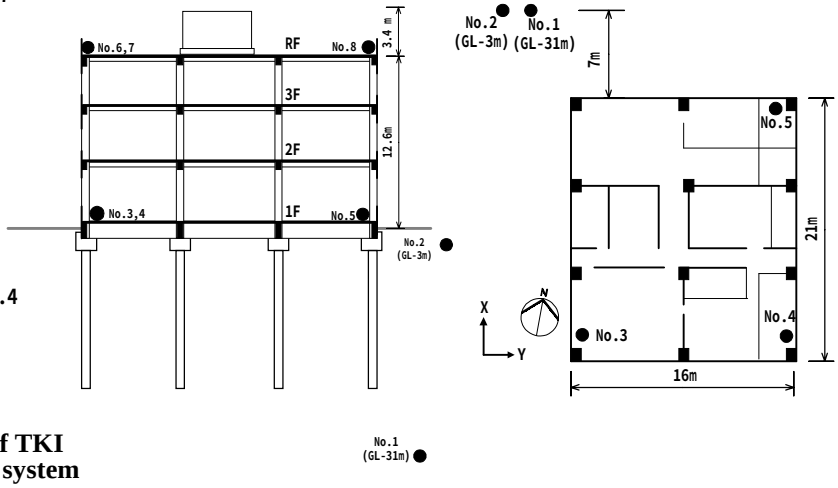


**(a)Vertical view** **(b)Plane view**

**Figure A-2.2: Sensor configuration**

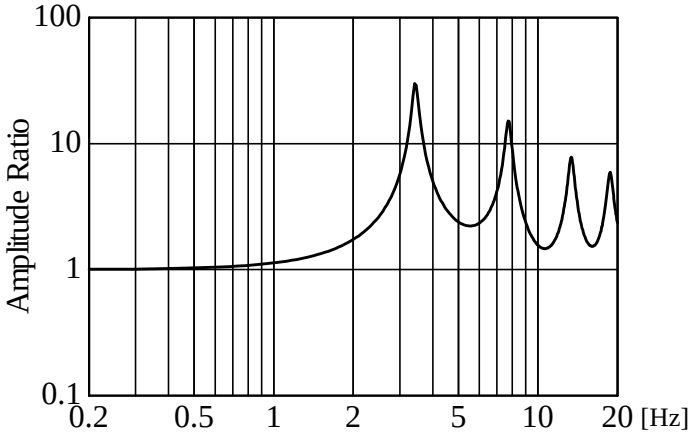


**Figure A-2.3 Transfer function of surface soil layers**

**Table A-2.1: Structure of surface soils**

| No. | *H* (m) | *D* (m) | *Vs* (m/s) | $\rho$ (t/m3) | Soil type |
|---|---|---|---|---|---|
| 1 | 3.0 | 3.0 | 120 | 1.65 | Silty sand |
| 2 | 2.0 | 5.0 | 140 | 1.65 | Silty sand |
| 3 | 5.0 | 10.0 | 250 | 1.80 | Fine sand |
| 4 | 5.0 | 15.0 | 280 | 1.80 | Fine sand |
| 5 | 5.0 | 20.0 | 300 | 1.80 | Fine sand |
| 6 | 11.0 | 31.0 | 500 | 1.90 | Fine sand |

**3. TDI**

Earthquake observation has been carried out to investigate dynamic soil-structure interaction behavior since September 1988. Sensor configuration, cross-section and plan of the building are summarized in Figure A-3.1. The soil constants round the building are shown in Table A-3.1. Geological structure consists of soft alluvial deposits above three meters, underlying hard soil deposits above eight meters and underlying diluvial deposits. About eight meters below the ground surface, there exists a firm diluvial deposit, which is selected as the bearing stratum of the building.

Earthquakes are observed with arrays set up inside the building and those set up vertically in the ground about 180 meters from the building, respectively. Accelerometers are installed in the building (3 sets, 6 components), in the ground about 180 meters from the building (4 sets,12 components) as shown in Figure A-3.1. The building is a reinforced concrete structure supported by cast-in-place concrete pile foundations with a about 22.5m height and a typical floor area of 22.5m×15m. The first natural frequencies of the building in the X- and Y-directions are 3.5 and 3.35 Hz, respectively. In the analysis, on the assumption that the soil consists of a multiple-layer horizontal formation, the amplitude characteristics are calculated by the one dimensional wave propagation theory. The transfer characteristics obtained from the soil model is shown in Figure A-3.2. As shown in this figure, predominance is shown at frequencies 0.8Hz, 2.0Hz, 4.0Hz, 5.0Hz and 6.0Hz above. Predominant frequencies in higher modes of oscillation having a frequency of 4.0Hz or above are produced in shallow layers at GL-17m or above.

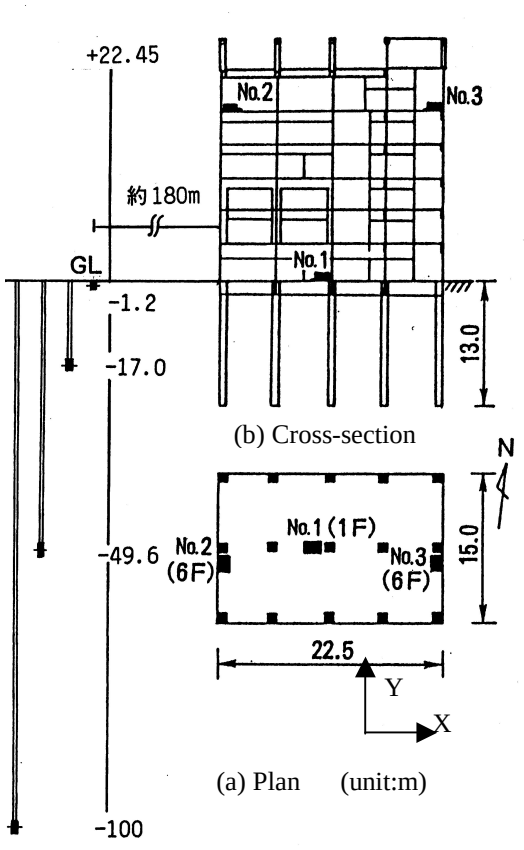


**Figure A-3.1 Outline of the building structure and Sensor configuration**

**Table A-3.1. Data of soil profile**

| Sensor configuration | H (m) | Vs (m/s) | ρ ($t/m^3$) | Soil Type |
|---|---|---|---|---|
| GL-1.2m | 1.2 | 120 | 1.57 | Loam |
| | 1.8 | 120 | 1.57 | Clay&Clayey sand |
| | 5.0 | 218 | 1.57 | Clayey sand |
| GL-17m | 9.0 | 244 | 1.74 | Fine sand |
| | 5.0 | 244 | 1.74 | Middle sand |
| | 6.0 | 193 | 1.63 | Silt |
| | 17.0 | 267 | 1.78 | Silt & middle sand |
| L-49.6m | 4.6 | 484 | 1.82 | Gravel &Fine sand |
| | 4.4 | 484 | 1.82 | Fine sand |
| | 17.0 | 310 | 1.80 | Silt & Gravel |
| | 12.0 | 330 | 1.85 | Fine sand |
| | 8.0 | 270 | 1.60 | Silt & middle sand |
| GL-100m | 9.0 | 610 | 2.00 | Gravel |
| | ∞ | 610 | 2.00 | Gravel |

where, H: Thickness, Vs: Shear wave velocity and ρ :Density.
$h(f)=h_0 \times f^{-\alpha}$:Frequency dependent damping factor

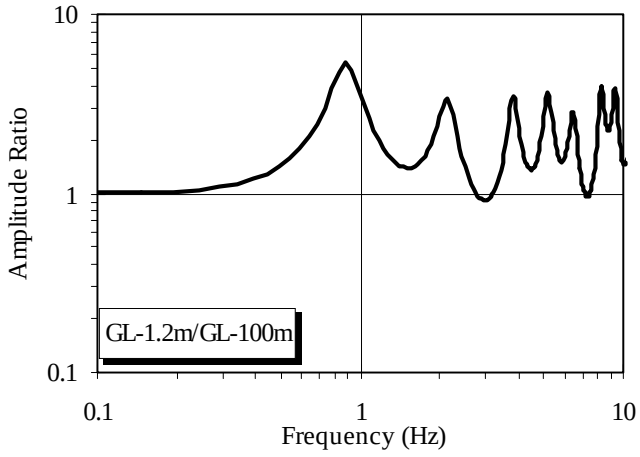


**Figure A-3.2 Transfer function of surface soil**

**4. KII**

**a)Structure**
- The Building "Konoike Institute" (see Picture A-4.1) is an office building as research institute.
- Superstructure of 3-stories is RC-rahmen frames and walls with base-isolation system shown in Figure A-4.1(1).
- Base-isolation devices are rubber bearings, steel damper, and lead damper shown in Figure A-4.1(2).
- Building has atrium for lightning at center of building, so multi-floor model is used to seismic response analysis in seismic design.

**b)Soil**
- Soil Condition is shown in Figure A-4.2.
- Horizontal predominant frequency on ground is 1.7Hz by small earthquake and tremors shown in Figure A-4.3(up).
- Calculated eigen frequencies of soil surface are in accordance to results of observation shown in Figure A-4.3(left).

**c)Observation**
- Strong motion observation is being carried out from Sept. 1998.
- Sensor layout is shown in Figure A-4.4.

**Picture A-4.1 View of Building F**

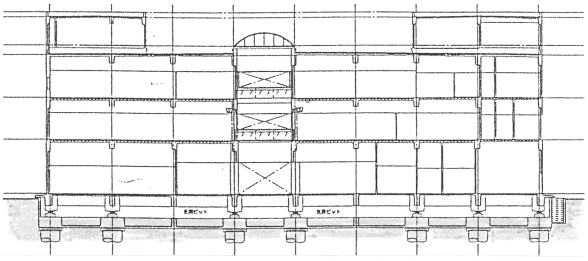

**(1) South-North Elevation**

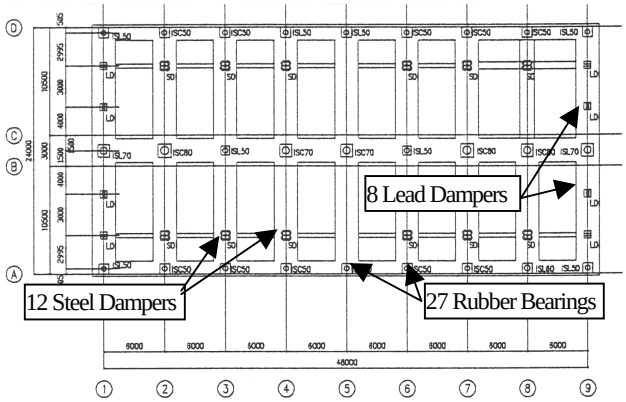


**(2) Base Isolation Devices Arrangement**

**Figure A-4.1 Summary of Structure**

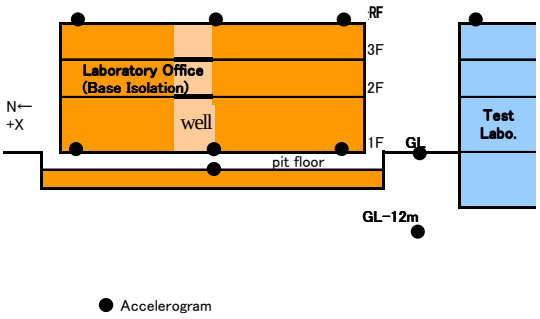


**Figure A-4.4 Sensor layout**

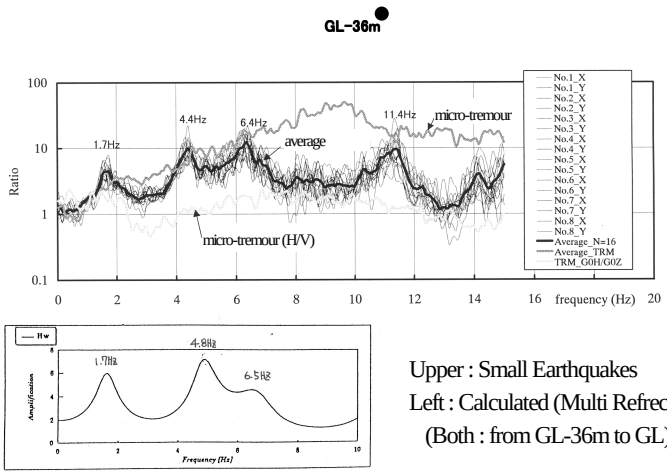


Upper : Small Earthquakes
Left : Calculated (Multi Refrection)
(Both : from GL-36m to GL)

**Figure A-4.3 Soil Dyanamic Characteristics**

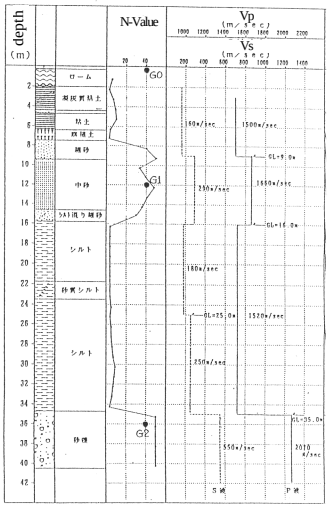


**Figure A-4.2 Soil Condition**

## 5. AOB

Figure A-5.1 shows the cross-section of the building at AOB site. The building is 7-story and reinforced concrete frame-wall building, and is seismically isolated structure with spread foundation (mat foundation). The isolation devices are laminated rubbers, steel-bar dampers, and lead dampers, which are set up on the basement floor. Sensor configuration is shown in Figure A-5.1, and the acceleogram sensors are installed at 5 locations. 1 sensor is on the foundation, 2 sensors are under the beam of the first floor, and 2 sensors are under the beam of the roof floor.

The profile of surface soil layers is shown in Table A-5.2, and the transfer functions for shear waves between at ground surface and at the depth of 38m is shown in Figure A-5.2. The figure shows predominant frequency of 6.3 Hz.

The system has 20bit A/D converter, IC card storages. The sampling frequency is 100Hz, the Acceleration range is $\pm 20.0$ m/s$^2$, and triggering logic disjunction of the component on the foundation.

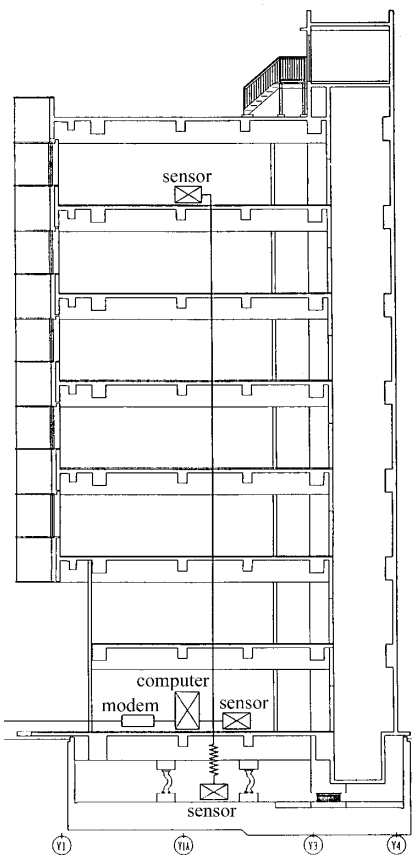


**Figure A-5.1 Sensor configuration**

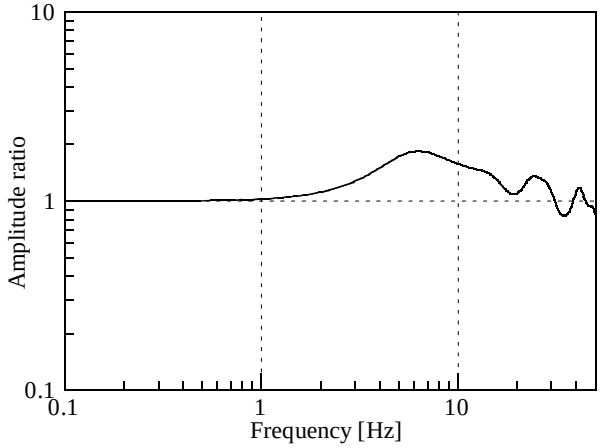


**Figure A-5.2 Transfer function of surface soil layers**

**Table 2. Structure of surface soil layers**

| No. | H (m) | D (m) | Vs (m/s) | ρ (g/cm$^3$) | Soil Type |
|---|---|---|---|---|---|
| 1 | 4.0 | 6.0 | 345 | 1.750 | Clay mixed sand gravel |
| 2 | 4.0 | 10.0 | 345 | 1.950 | Gravely clay |
| 3 | 8.0 | 18.0 | 495 | 2.075 | Tuff |
| 4 | 6.0 | 24.0 | 585 | 2.150 | Mudstone |
| 5 | 14.0 | 38.0 | 660 | 2.288 | Tuff and mudstone |
| 6 | 12.0 | 50.0 | 715 | 2.238 | Tuff and mudstone |

## 6. MST

Figure A-6.1 shows MST site recording system that has been installed since February 1991 by HAZAMA Corporation. Earthquake motions of a pile-supported 21-story residential building, which is constructed on soft soil, are observed. The building is a RC structure with SC and PHC pile foundation (40 sets of four piles, i.e. 160 piles).

The acceleration-type seismograms are installed at 10 locations (25 channels) and two of these locations have also velocity-type seismograms (4 channels). The strain sensors are installed at 7 sections of a centrally located pile, and a pore-water pressure sensor is installed in a sand layer (GL-8m) at the surface ground. All the sensors are connected to the recording equipment in an earthquake observation room. The system has 40-channels 16bits A-D converter and a MT storage. The sampling frequency is 100Hz. The dynamic ranges is ±1g and the triggering logic is disjunction (OR) of 3 components on -67m ground level in depth. Figure A-6.2 shows soil profiles of the ground. The soil type of this site is Type 3 (soft soil) in the soil description of the Building Standard Law of Japan. Figure A-6.3 shows a theoretical amplification function of the surface ground and the first predominant frequency is about 0.9 Hz.

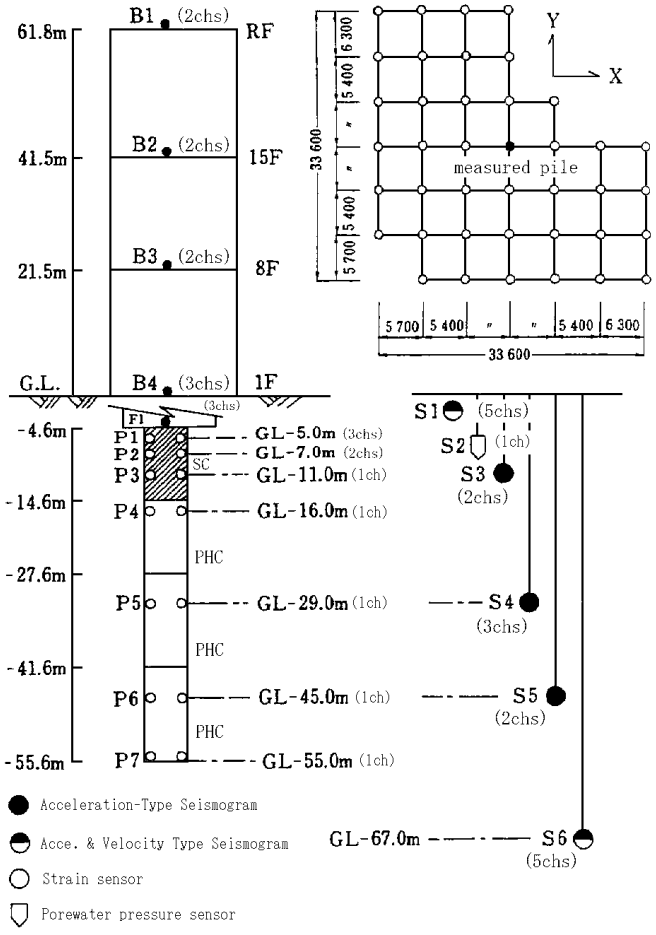


**Figure A-6.1 Sensor Configuration**

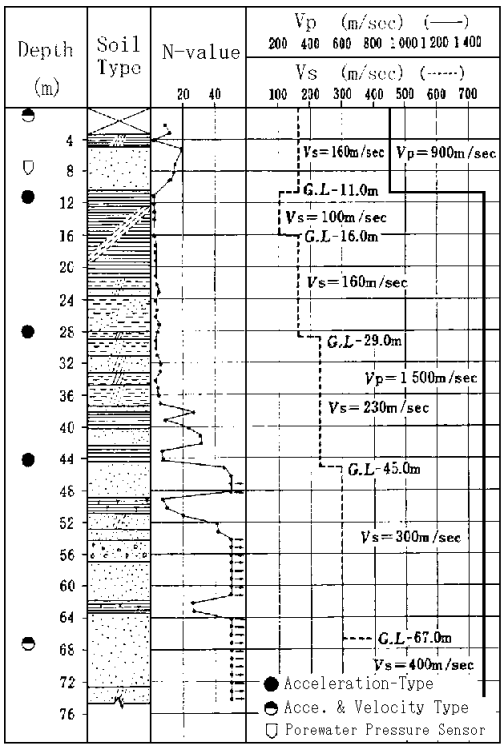


**Figure A-6.2 Soil Profile and P-S Logging**

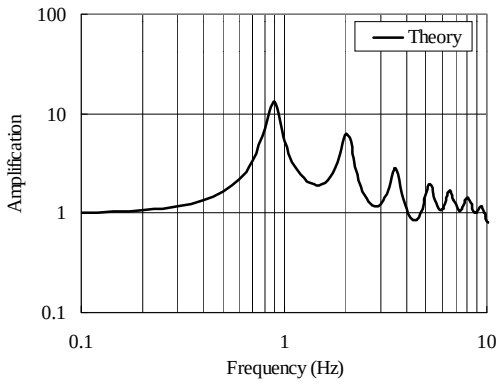


**Figure A-6.3 Absolute amplification function of the surface ground (hysteretic damping model)**

## 7. TKM

a)Structure
- The building is a high-rise apartment completed at 1989.
- The structure is RC-Rahmen Frames(Moment Resistance Frames).
- Picture A-7.1 shows the shape of tower type structure.
- Figure A-7.1(1)-(4) show each east-west elevation, key plan, 1st-floor plan, pile arrangement, respectively.
- TKM site received earthquake response by “1995 Hyogo-ken Nanbu Earthquake”. PGA reached 2.67m/s$^2$, and maximum deformation angle of whole height was about 1/150.

b)Soil
- Ground condition is shown in Figure A-7.2 with results of vibration velocity characteristics.
- Horizontal predominant frequency on ground is 1.5Hz in micro-tremours measurement.

c)Observation
- Strong Motion Observation has worked from Oct. 1989.
- Sensors are located at free surface ground, bottom of pile, 1st-floor, mid-floor and roof floor, shown Figure A-7.1.
- Sensors are all accelerometers which have frequency range 0.1 to 30Hz flatness.

**Picture A-6.1 View of the building**

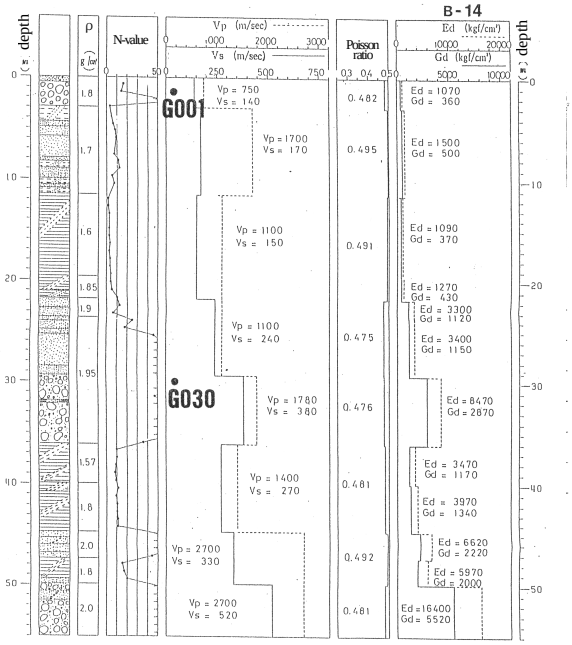


**Figure A-7.2 Soil Condition**

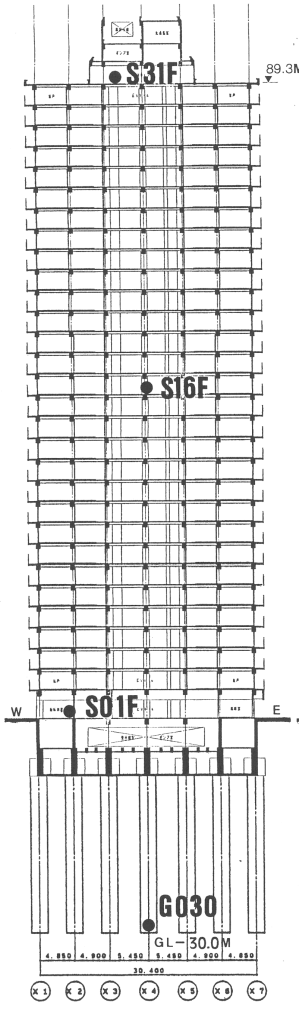


**(1)East-West Elevation**

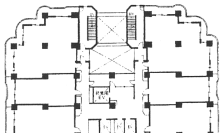


**(2) Key Plan**

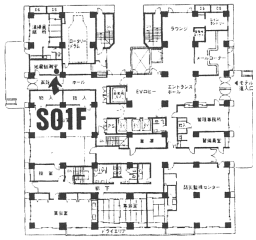


**(3) 1st Floor**

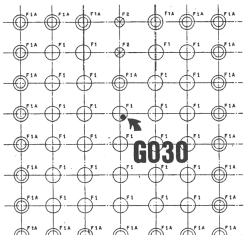


**(4) Pile arrangement**

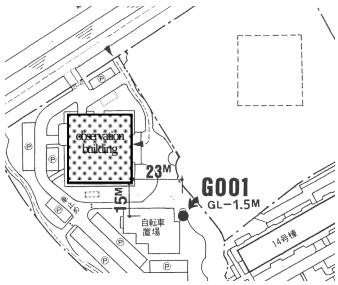


**(5) Sensor of ground surface**

**Figure A-7.1 Structure and sensors layout**

## 8. HRM

Figure A-8.1 shows the cross-section and plans of the building at HRM site. The building consists of two different height ridges, which are connected at basement floors, and is used for residual complex. CFT (concrete filled tube) columns are used over 2nd floor, and both cast-in-place concrete pile and the diaphragm wall foundation are used as foundation.

The accelerogram sensors are installed at 15 locations (36 channels) and the 4 strain meters are installed on the basement floor columns. Sensor configuration is also shown in Figure A-8.1. 2 sensors are set up on the ground at 1m and 34m in depth, 6 sensors in piles and diaphragm wall foundation, 5 sensors at the second basement, 2 sensors at 25$^{th}$ floor and 51$^{st}$ floor.

Surface soil profile at HRM is shown in Table A-8.1, and the transfer function for shear waves between at ground surface and at the depth of 35m is shown in Figure A-8.2. The figure shows predominant frequency of 1.6 Hz.

The system has 40-channels 16bit A-D converter, IC card storages. The sampling frequency is 100Hz, the dynamic range is ±1g, and triggering logic disjunction (OR) of three components on the 34m ground level in depth.

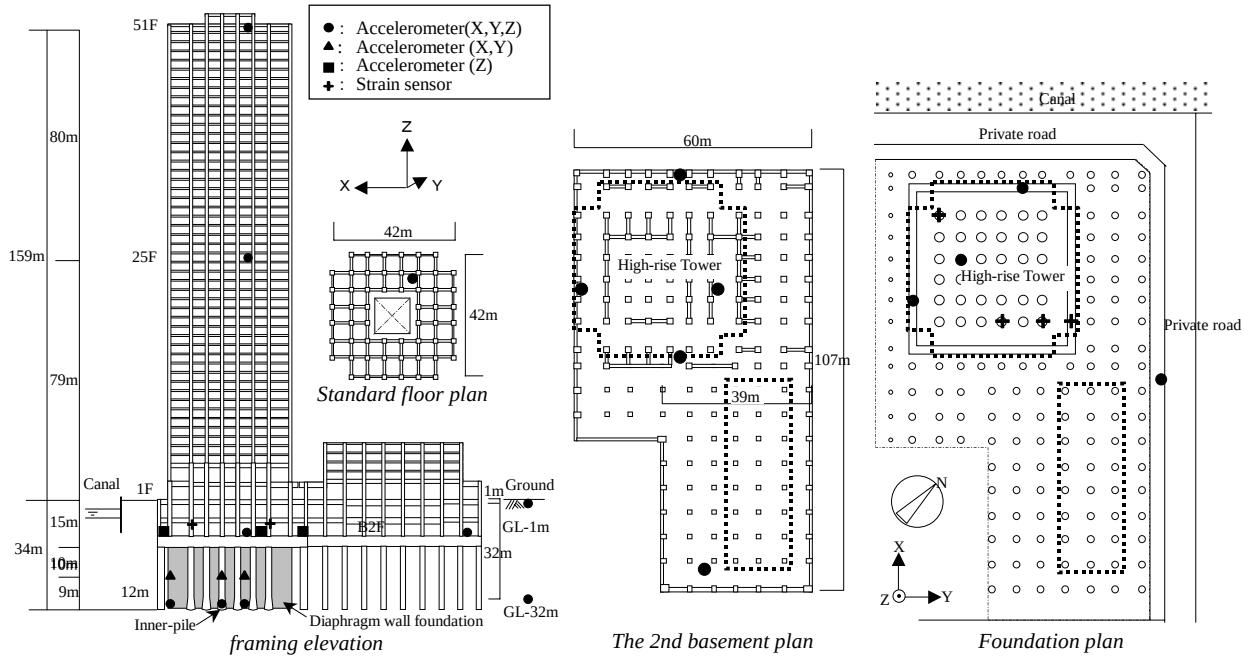


**Figure A-8.1 Sensor Configuration**

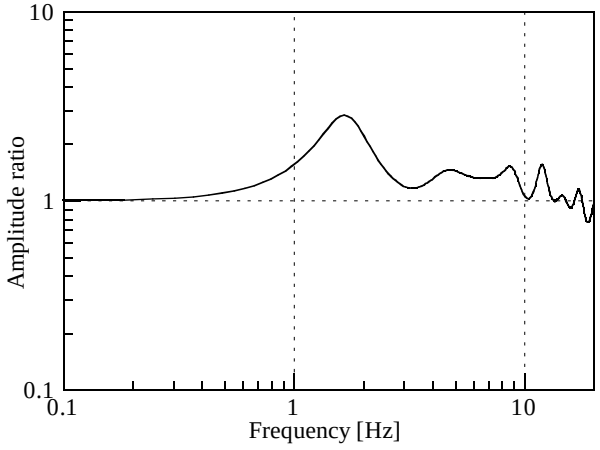


**Figure A-8.2 Transfer function of surface soil layers**

**Table A-8.1 Structure of surface soil layers**

| No. | H(m) | D(m) | Vs(m/s) | ρ (t/m$^3$) | Soil Type |
|---|---|---|---|---|---|
| 1 | 3.9 | 3.9 | 140 | 1.70 | Sand |
| 2 | 6.3 | 2.4 | 130 | 1.77 | Silt |
| 3 | 12.6 | 6.3 | 110 | 1.77 | Silty Clay |
| 4 | 17.6 | 5.0 | 150 | 1.77 | Clay |
| 5 | 19.8 | 2.2 | 200 | 1.77 | Clay |
| 6 | 21.5 | 1.7 | 220 | 1.90 | Sand |
| 7 | 25.7 | 4.2 | 280 | 1.90 | Sand |
| 8 | 27.6 | 1.9 | 380 | 1.90 | Silty Sand |
| 9 | 29.6 | 2.0 | 230 | 1.90 | Sandy Silt |
| 10 | | | 380 | 1.90 | Sand |

H: Thickness, D: Depth, Vs: S-wave Velocity, ρ :Density

**" CHARACTERISTICS OF SEISMIC MOTION OF THE BUILDING AND GROUND " in BRIC**

**IZURU OKAWA (the chairman of the investigation)**
*Building Research Institute Ministry of Land, Infrastructure and Transport*
*Tachihara-1, Tsukuba-shi, Ibaraki-ken, 305-0802*
*E-mail : okawa@kenken.go.jp*

**TOSHIHIDE KASHIMA**
*Building Research Institute Ministry of Land, Infrastructure and Transport*
*Tachihara-1, Tsukuba-shi, Ibaraki-ken, 305-0802*
*E-mail : kashima@kenken.go.jp*

**SHIN KOYAMA**
*Building Research Institute Ministry of Land, Infrastructure and Transport*
*Tachihara-1, Tsukuba-shi, Ibaraki-ken, 305-0802*
*E-mail : koyama@kenken.go.jp*

**NOBUAKI HANAI**
*Technology Research Laboratory, Ohki Corp.*
*Shiroi-Dai2-Kogyodanchi, Hiratsuka, Shiroi-cho, Imba-gun, Chiba-ken, 270-1402*
*E-mail : hanai@ohki.co.jp*

**KENJI YASUI**
*Technical Research Institute, Okumura Corp.*
*387, Ohsuna, Tsukuba-shi, Ibaraki-ken, 300-2612*
*E-mail : oku07274@gm.okumuragumi.co.jp*

**HIROSHI MATSUZAKI**
*Technical Research & Development Institute, Kumagaigumi Co.,LTD.*
*1043, Onigakubo, Tsukuba-shi, Ibaraki-ken, 300-2651*
*E-mail : hmatsuza@ku.kumagaigumi.co.jp*

**ATSUSHI FUJII**
*Research Institute of Technology, Konoike Construction Co.,LTD.*
*1-20-1, Sakura, Tsukuba-shi, Ibaraki-ken, 305-0003*
*E-mail : fujii_as@konoike.co.jp*

**MORIMASA WATAKABE**
*Technical Research Institute, Toda Corp.*
*315, Kaname, Tsukuba-shi, Ibaraki-ken, 300-2622*
*E-mail : morimasa.watakabe@toda.co.jp*

**MITOSHI YASUI**
*Technical Research Institute, Toda Corp.*
*6-1, Hacchobori, 4-chome, Chuo-ku, Tokyo, 104-0032*
*E-mail : mitoshi.yasui@toda.co.jp*

**SHOZO SHIRINASHIHAMA**
*Technical Research Institute, Tekken Corp.*
*9-1, Shin-izumi, Narita-shi, Chiba-ken, 286-0825*
*E-mail: shozo-shirinashihama@tekken.co.jp*

**RYOICHI KANNO**
*Technical Research Institute, Toyo Construction Co.,LTD.*
*1033-1, Miho-mura, Inashiki-gun, Ibaraki-ken, 300-0424*
*E-mail : r-kanno@toyo-const.co.jp*

**SHIGEKI SAKAI**
*Technical Research Institute, Hazama Corp.*
*515-1,Karima, Tsukuba-shi, Ibaraki-ken, 305-0822*
*E-mail : ssakai@hazama.co.jp*

**TAKASHI KATO**
*Technical Research Institute, Hazama Corp.*
*515-1,Karima, Tsukuba-shi, Ibaraki-ken, 305-0822*
*E-mail : takakato@hazama.co.jp*

**KUNIAKI YAMAGISHI**
*aforenamed*